IEEE Access
Multidisciplinary | Rapid Review | Open Access Journal

Received January 14, 2022, accepted February 1, 2022, date of publication February 8, 2022, date of current version February 28, 2022.

Digital Object Identifier 10.1109/ACCESS.2022.3150037

Large-Aperture Metamaterial Lens Antenna for Multi-Layer MIMO Transmission for 6G

JAEHYUN LEE[1], (Member, IEEE), HOGYEOM KIM[2], (Graduate Student Member, IEEE), AND JUNGSUEK OH[2], (Senior Member, IEEE)

[1]6G Research Team, Samsung Research (Samsung Electronics), Seoul 06765, Republic of Korea
[2]Institute of New Media and Communications, Seoul National University, Seoul 08826, Republic of Korea

Corresponding author: Jaehyun Lee (jhyun730.lee@samsung.com)

This work is supported by SAMSUNG Research, Samsung Electronics Co., Ltd.

ABSTRACT A metamaterial lens refers to a planar structure having multiple metamaterial unit cells capable of manipulating electromagnetic waves to improve antenna gains by changing their shape, geometry, size, or orientation. In this paper, we propose a large-aperture metamaterial lens antenna (MLA) designed to improve the gain of multiple beams emitted from a linear feed antenna array, taking multi-layer transmission into account. A new channel model incorporating MLA is presented to evaluate the performance of the proposed MLA on beam gain and system throughput gain. The channel model is derived by decomposing the entire propagation channel from the transmit antenna to the receive antenna through metamaterial lens into five serial channels. The measurement results of the MLA prototype prove that the channel model is valid to reflect the actual multiple beam patterns. Simulation results based on the channel model show that a single large-aperture MLA can achieve beam gain of up to 14 dB compared to the case without a lens. Finally, by adopting the proposed large-aperture MLA, it is shown through system-level simulation that the throughput of user equipment is increased on cellular networks.

INDEX TERMS Lens antenna, metamaterial, metasurface, MIMO, 6G.

I. INTRODUCTION

In order to meet the increasing demands for data rate in wireless communications, mobile communication systems are evolving toward utilizing higher frequencies such as millimeter wave (mmWave) and terahertz (THz) bands (see Fig.1) [1], [2]. Both mmWave and THz communication systems can utilize extremely large bandwidth and can therefore boost peak data rates in 6G. However, electromagnetic (EM) waves at higher spectrum experience orders-of-magnitude more path loss than those at much lower spectrum at the same propagation distance. Specifically, the physical relation between wireless communication devices is described by the fundamental equation in telecommunication engineering, called *Friis transmission equation*, which is given as

$$P_r = (\frac{\lambda}{4\pi d})^2 G_t G_r P_t \tag{1}$$

where P_r [W] is the received power at the distance d [m], λ [m] is the wavelength of the EM wave, G_t and G_r is the transmit (TX) and receive (RX) antenna gain, respectively, and P_t [W] is the transmit power of a TX antenna. Since λ is inversely proportional to the frequency f, i.e., $f = \lambda/c$ where c is the speed of EM waves including light, the received power P_r at a certain transmission distance d decreases rapidly, inversely proportional to the square of the frequency, i.e., $P_r \propto 1/f^2$. Governed by (1), one of the practical solutions

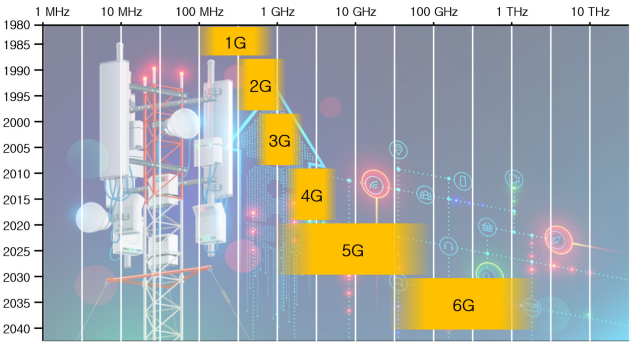

FIGURE 1. Mobile cellular spectrum–from the first generation (1G) in the 1980s to the sixth generation (6G) that is predicted around 2030s.

The associate editor coordinating the review of this manuscript and approving it for publication was Shah Nawaz Burokur.

to exploit the broad spectrum of the mmWave and THz bands in cellular networks is either to increase the input transmit power P_t or to improve the TX and RX antenna gains G_t and G_r. However, P_t cannot be increased indefinitely due to radio regulations to protect human body from hazardous radio waves and the power efficiency required for cellular networks. Therefore, an efficient way to overcome the intrinsic high loss of received power of mmWave and THz waves is to increase G_t and G_r at all costs [3].

On the other hand, there is also a promising way to increase antenna gain thanks to its high-frequency characteristics. As the frequency increases, the physical size of the antenna element decreases. At mmWave and THz frequencies, the wavelengths are so short that hundreds of antenna elements can be designed on the same physical space where only a few elements are currently possible. This allows a large number of antenna elements to be packaged within a reasonable form factor to take advantage of higher antenna gain. 5G, a state-of-the-art mobile communication technology standard that was first commercialized in 2019, has been growing based on this multiple-antenna technology, also known as massive multiple-input and multiple-output (MIMO) [4]. With massive MIMO technology, 5G achieves high beamforming gain that would secure the coverage and reduce interference of the system because the beamwidth of massive MIMO becomes much narrower than before.

Massive MIMO technology promises significant antenna gain, but it also entails new challenges associated with the practical difficulties of densely deploying a very large number of antenna elements [5]. For example, a large amount of antenna elements incurs tremendous hardware complexity, including the cost associated with radio frequency (RF) chains composed of mixers, amplifiers, D/A and A/D converters at each of the TX/RX antennas. Increased total energy consumption by using multiple RF chains boils down to a banal method of increasing P_t as before, unlike the initial purpose of increasing antenna gain by massive MIMO.

To reduce the number of required antennas and corresponding RF chains while maintaining high beamforming gain, an electromagnetic lens antenna (ELA) with a reasonable number of antenna elements has been proposed [5]–[7]. With a carefully designed shape, EM lenses made of dielectric material can refract incident EM wave toward a desired direction so that the transmitted energy can be concentrated in a targeted area. Thus, ELA can focus on dispersive energy and provide spatial separation of multipaths to improve the performance of cellular networks. However, dielectric EM lenses are difficult to integrate with multiple antenna techniques due to their bulky size, high insertion loss, and long focal lengths to control the beam gain.

Instead of dielectric ELA, metamaterial lens antenna (MLA) structures have attracted much attention in recent years [8]–[10]. Metamaterials are defined as artificial composites that obtain electrical properties from their structure rather than their constituent materials. Various fields such as antennas, lenses, transmission lines, and electromagnetic band gaps are actively studied as applications that utilize the electrical properties of metamaterials [11]–[14]. In terms of EM theory, it can change (relative) electric permittivity ϵ and magnetic permeability μ. And the refractive index n of a material is the square root of the product of ϵ and μ, i.e., $n = \sqrt{\epsilon\mu}$. Thus, just as ELA changes the directions of refracted EM waves with the thickness of the dielectric medium, one can refract impinging EM waves by changing the physical structures of the metamaterial. In particular, by densely disposing of metamaterial unit cells with different ϵ and μ on a plane, one can design a planar metamaterial lens with superior lens properties such as smaller size, lower insertion loss, and shorter focal length compared to dielectric ones [15]. There have been several studies on MLA to achieve beam gain from a single antenna [9], but few have been considered on the multi-layer transmission with multiple-antenna. Because MLA research is still in its infancy, existing studies have been focused on the realization of the single-fed MLA [10].

This paper proposes a large-aperture MLA design for multi-layer MIMO transmission for 6G. The design process of the proposed MLA is as follows: First, the radiation pattern of a feed antenna is determined. Based on the received power from the feed antenna, each MLA unit cell is designed to impede incoming EM waves to compose collimated beams with other unit cells. The phase offset values are determined by the meta channel, which includes the geometric modeling of MLA and EM wave propagation. Measurement and simulation results show that significant lens gains of up to 14 dB can be obtained in various beam directions by the lens prototype which is composed of 28 $\times$ 28 unit cells, within 50.4 mm $\times$ 50.4 mm size, operating at 28 GHz carrier frequency and 50 MHz bandwidth. [1] Therefore, it is possible to utilize the proposed large-aperture MLA to reduce the number of feed antenna elements and RF chains required to implement a large-scale MIMO system while maintaining high beamforming gain. In addition, the network performance improvement was verified by applying the proposed MLA design to the system-level simulation considering the mmWave band propagation channel. Thus, the proposed MLA can be utilized as a new antenna system for 6G cellular networks to mitigate high path loss and fading and ensure sufficient received signal powers.

The rest of paper is organized as follows. We first briefly introduce theoretical backgrounds of metamaterial lens and metamaterial unit cell design in Section II. Next, Section III introduces the proposed MLA system design and a new channel modeling method that encompasses the novel properties of MLA. Section IV shows the simulation results to prove the throughput gain obtained from the proposed multi-layer transmission scheme with the proposed MLA structure, and Section V concludes the paper.

[1] Since the main purpose of this paper is to identify the possibility of increasing lens gain by the designed metamaterial unit cells, the efficiency of the metamaterial lens is not considered. Lens efficiency can be calculated by measuring the radiation pattern of the anechoic chamber, which is beyond the scope of this article.

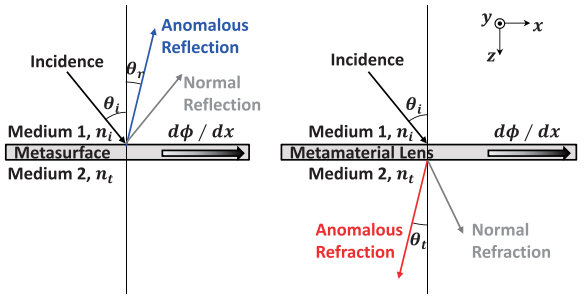

FIGURE 2. The generalized law of reflection and refraction.

II. THEORETICAL BACKGROUNDS

A. PRINCIPLE OF METAMATERIAL LENS

The principle of metamaterial lenses is represented by the generalized law of reflection and refraction, initially introduced in 2011 [16], [17]. In a nutshell, it describes the relation between the incident and refracted angles of an EM wave across the metamaterial when the one-dimensional metamaterial unit cell has a negligible thickness along the z-axis and a phase discontinuity $d\phi(x)/dx$ along the x-axis, as shown in Fig. 2. The formula is given as follows:

$$n_t \sin(\theta_t) - n_i \sin(\theta_i) = \frac{\lambda}{2\pi} \frac{d\phi(x)}{dx} \tag{2}$$

where θ_t, θ_i, n_t, n_i are angles and refractive indexes of transmitted and incident mediums, respectively. Note that without phase discontinuity introduced by the metamaterial (i.e., if $d\phi(x)/dx = 0$), (2) is equivalent to Snell's law of refraction[2] following traditional geometric optics. It implies that the refracted wave can have an arbitrary direction θ_t, provided that a gradient of phase discontinuity along interface is properly implemented as shown Fig. 2.

Fig. 3 depicts the reciprocal property of a metamaterial lens. The left subfigure illustrates that a spherical wave from a TX feed antenna forms a directive plane wave by the metamaterial. This beam controllability is attributed to the unit cells with different phase offsets ϕ_{meta}, depending on the radial distance d to the focal axis through antenna and the center of metamaterial lens. According to the Huygens-Fresnel principle, the equiphase wave fronts can be generated by constructive interference of phase-delayed spherical waves [18]. The right subfigure illustrates the reverse phenomenon. From the plane wave generated by a feed antenna array,[3] the metamaterial concentrates the EM wave by applying phase offsets. In this paper, it is assumed that the phase and amplitude of spherical waves from multiple antennas interfere each other at the metamaterial lens, and the unit cells act as phase shifters that are spatially distributed to enhance different beam directions to take advantage of the MLA structure.

[2]Snell's law states that the ratio of the sines of the angles of incidence and refraction is equivalent to the reciprocal of the ratio of the indices of refraction: $n_i \sin(\theta_i) = n_t \sin(\theta_t)$

[3]In the following example and after, the reactive near-field of the EM wave is negligible, since only the distances within far-field condition (further than Fraunhofer distance) are considered, i.e., $d > d_F = (2D^2)/\lambda$, where D is the antenna dimension.

B. IMPLEMENTATION OF METAMATERIAL UNIT CELLS

Although this paper focuses on the benefit of multi-layer transmission with a large-aperture MLA structure for cellular networks rather than the physical implementation of metamaterial, we would like to briefly introduce some of the published metamaterial unit cell designs.

In practice, metamaterial unit cells induce discrete phase delays (or phase offsets) to the incoming EM waves depending on their physical characteristics. To change phase offsets, unit cells consist of a single or multi-layer planar structure by periodically printing sub-wavelength metal structures on a dielectric substrate [19]–[21]. For example, there are several implementations of single or multi-layered Jerusalem cross-shaped metamaterial unit cell [9], [22]. Split-ring resonator structure with different widths and lengths of metal are also feasible to constitute the metamaterial lens [23], [24]. Note that these structures are usually much smaller than the corresponding wavelength of EM waves, normally tenth of wavelength. Recently, not only the experimental prototypes but also metamaterial lenses are being manufactured on printed circuit boards (PCBs) [25], so mass production is expected to be possible soon.

A remaining problem with the MLA structure is that there is a quantization loss due to the discrete form factor of metamaterial unit cell. This can be addressed by diversifying the unit cell design to have an arbitrary phase shift. For example, some of early studies show that there are 17 different design of metamaterial unit cells by changing their width, length, diameter of the structure, which results in considerable quantization losses [26]. Utilizing different type of dielectric materials could be another option to change the phase-delaying properties of the unit cells. Current research trends are mainly focused on a new design of metamaterial unit cells to enhance the single antenna-fed EM waves to only a certain direction, which is normally boresight direction. However, the research trend of MLA is gradually changing from single-layer transmission to the multi-layer transmission to acquire both beamforming gain and spatial multiplexing gain, which is a main contribution of our paper.

III. METAMATERIAL LENS ANTENNA SYSTEM

A. SYSTEM DESIGN

Fig. 4 shows the proposed MLA TX structure[4] applied for $S \times U$ multi-antenna transmission system at a base station (BS) studied in this paper. The modulated symbols are mapped to codeword with layer according to the channel state information feedback from the receiver. The precoding process is done by multiplying the precoding matrix $\boldsymbol{P}$ to the given codeword vector. The waveform generation is done by following multiplexing schemes such as OFDM. The dotted box in Fig. 4 is the main part of the proposed MLA structure in this article, which contains the TX feed antennas (triangles)

[4]In the proposed scheme, the beam patterns with different direction are generated in spatially distributed metamaterial unit cells. Thus, it actually radiates from different locations, but is conceptually illustrated to help understanding.

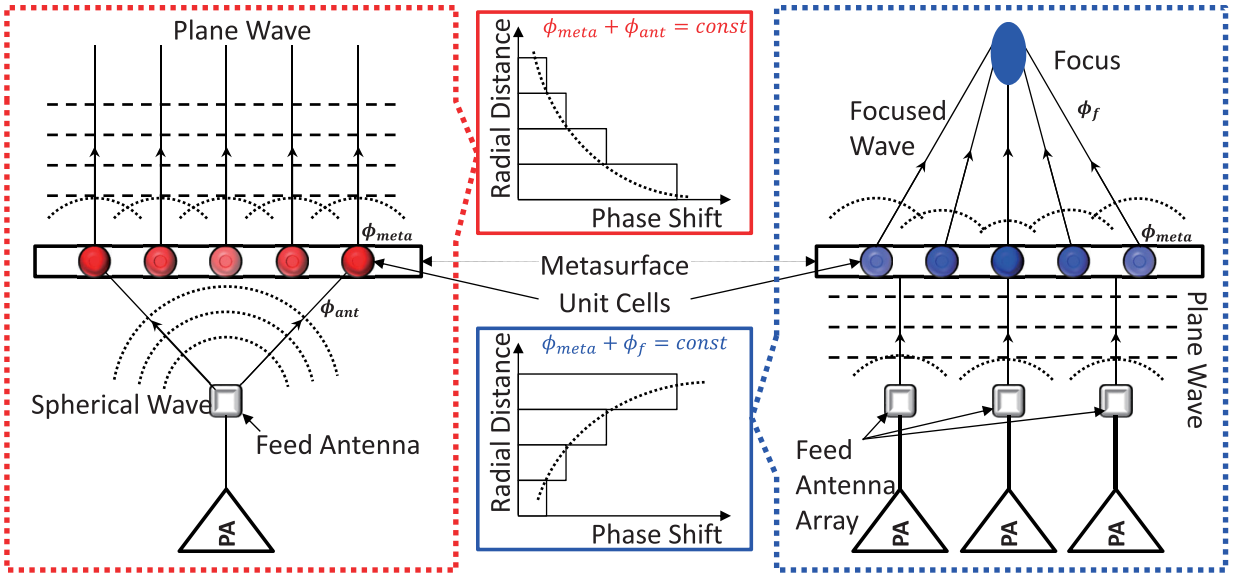

FIGURE 3. Principle of metamaterial lens antenna. Left subfigure shows that a spherical wave radiated from feed antenna is transformed to a plane wave by metamaterial unit cells (red circles) which have different phase shifting properties. Right subfigure shows the reciprocal phenomenon by metamaterial lens to form a focused wave from a plane wave radiated from feed antenna array.

and the metamaterial lens (rectangle). Assuming that $\vec{y}$ is an $U \times 1$ RX signal vector at an user equipment (UE), it can be expressed as

$$\vec{y} = \boldsymbol{H}\boldsymbol{P}\vec{x} + \vec{n} \tag{3}$$

where $\boldsymbol{H}$ is the $U \times S$ channel matrix between TX and RX antennas, $\boldsymbol{P}$ is a precoding matrix,[5] $\vec{d}$ is a modulated symbol vector, $\vec{x}$ is a codeword vector, and $\vec{n}$ is an additive white Gaussian noise vector. From (3), the proposed MLA structure changes the previous MIMO channel matrix $\boldsymbol{H}$ into MLA-incorporated channel matrix $\boldsymbol{H}_{meta}$ representing entire propagation channel from the feed TX antenna to the RX antenna, which will be described in detail in the following subsections. Note that the blue ellipse represents the first beamforming pattern by a precoding $\boldsymbol{P}$, and the red ellipse represents the enhanced beamforming pattern after the metamaterial lens.

B. MULTIPLE FEED ANTENNA MODELING

First, we model the radiation pattern of the feed antenna herein to derive a new channel model $\boldsymbol{H}_{meta}$ from the previous $\boldsymbol{H}$. Let $A_e(\theta, \phi)$ represent an antenna radiation pattern and measures the radiated power gain in all directions from a single antenna element. For example, an isotropic antenna has no power gain as the radiated power is the same in all directions, i.e., $A_e^{iso}(\theta, \phi) = 0$ dB. It is composed of elevation (vertical) and azimuth (horizontal) fairs, denoted by $A_{e,V}(\theta, \phi)$ and

[5]In this example, $\boldsymbol{P}$ represents a beamforming process to support multi-layer transmission in multi-antenna wireless communications. It is determined by BS considering channel state information (CSI) feedback from UE.

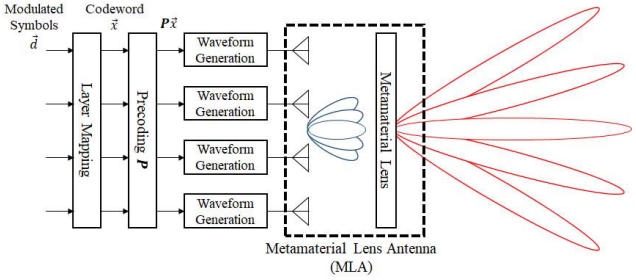

FIGURE 4. Proposed MLA structure.

$A_{e,H}(\theta, \phi)$, respectively, where θ is elevation angle and ϕ is the azimuth angle in spherical coordinate. Following third-generation partnership project (3GPP) technical report [27], the elevation radiation power pattern $A_e(\theta, \phi)$ in dB scale is modeled as

$$A_{e,V}(\theta, \phi = 0) = -\min\left(12\left(\frac{\theta - 90}{\theta_{3dB}}\right)^2, SLA_V\right) \tag{4}$$

where θ_{3dB} is the vertical half-power beamwidth, and SLA_V is 30 dB and 25 dB for TX and RX respectively, and is the side-lobe attenuation in vertical direction. Similarly, the azimuth radiation pattern $A_{e,H}(\theta, \phi)$is modeled as

$$A_{e,H}(\theta = 90, \phi) = -\min\left(12\left(\frac{\phi}{\phi_{3dB}}\right)^2, A_{\max}\right) \tag{5}$$

where ϕ_{3dB} the horizontal 3 dB beamwidth, and the maximum attenuation $A_{\max}$ is 30 dB and 25 dB for TX and RX, respectively. The combined 3D radiation power pattern $A_e(\theta, \phi)$ is

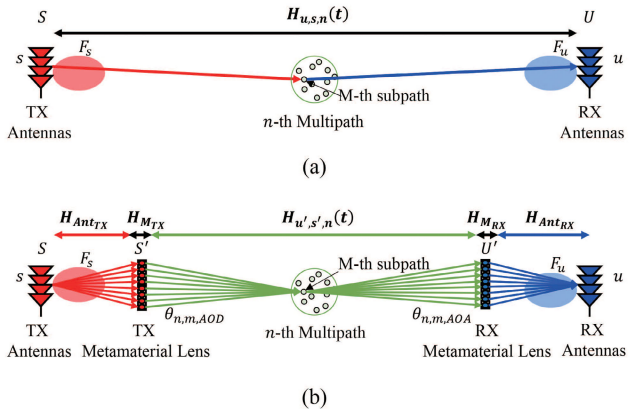

FIGURE 5. (a) MIMO channel without lens and (b) the proposed meta channel model with MLA structure on TX and RX.

obtained as

$$A_e(\theta,\phi) = G_{\max} - \min\left(-\left(A_{e,V}(\theta) + A_{e,H}(\phi)\right), A_m\right) \quad (6)$$

where $G_{\max}$ is the maximum directive gain of an antenna element.

In order to integrate the antenna radiation pattern with the channel model, radiation field pattern $F(\theta,\phi)$ is calculated in case of polarized antenna element assuming that ζ is the polarization slant angle in degree and are given by

$$\begin{aligned} F_\theta(\theta,\phi) &= \sqrt{A_e(\theta,\phi)}\cos(\zeta) \\ F_\phi(\theta,\phi) &= \sqrt{A_e(\theta,\phi)}\sin(\zeta) \end{aligned} \quad (7)$$

respectively. In the following channel models and simulations, we assume that ζ is $\pm 45°$ in order to model cross-polarized antenna elements. Note that if $\zeta = 0°$ corresponds to a purely vertically polarized antenna element, so we can model both co-polarized or cross-polarized antennas for any MLA design.

C. META CHANNEL

The meta channel $\boldsymbol{H}_{meta}$ refers to an integrated radio channel in which metamaterial lenses are applied to the TX and RX antenna arrays, so it can be decomposed into the following five consecutive channels:

$$\boldsymbol{H}_{meta} = \boldsymbol{H}_{Ant_{RX}}\boldsymbol{H}_{M_{RX}}\boldsymbol{H}_{UMa}\boldsymbol{H}_{M_{TX}}\boldsymbol{H}_{Ant_{TX}} \quad (8)$$

where 1) $\boldsymbol{H}_{Ant_{TX}}$ is the channel from a TX antenna to a TX metamaterial lens, 2) $\boldsymbol{H}_{M_{TX}}$ is the phase-delaying channel applied by a TX metamaterial lens, 3) $\boldsymbol{H}_{UMa}$ is the fast fading urban macrocell (UMa) channel from a TX metamaterial lens to the RX metamaterial lens, 4) $\boldsymbol{H}_{M_{RX}}$ is the phase-delaying channel applied by a RX metamaterial lens, and 5) $\boldsymbol{H}_{Ant_{RX}}$ is the channel from a RX metamaterial lens to a RX antenna, as shown in Fig. 5(b) compared with existing channels depicted in Fig. 5(a). Fig. 5 shows two figures: (a) MIMO channel with lens, and (b) MIMO channel with metamaterial lenses are inserted after the TX antennas and before the RX antennas, respectively. Due to the metamaterial unit cells, refracted rays are generated between the lens and they are depicted with green lines that can reflect, refract, or diffract by clusters generation M subpaths of N multipaths. Note that decomposing $\boldsymbol{H}_{meta}$ into independent channels is one of our major contributions. This is because, thanks to the proposed method, it is possible to design the MLA structure and simulate the effect of the designed MLA on the cellular network system. Lenses and feed antennas can also be designed jointly with geometric parameters such as distance, spacing, and phase delay of the metamaterial unit cell. This is explained in more detail below.

First, $\boldsymbol{H}_{Ant_{TX}}$ and $\boldsymbol{H}_{Ant_{RX}}$ are predetermined stationary channel because spatial variables such as the number of antennas, the number of metamaterial unit cells, and the distance between the antenna element and the metamaterial unit cell are fixed once the MLA is fabricated. In this assumption, the channel between antenna element $s \in S$ to the metasurface $s' \in S'$ can be given as

$$h_{s,s'} = \frac{1}{d_{s,s'}} e^{-jkd_{s,s'}} \times F_s(\theta_{s,s'}, \phi_{s,s'}) \quad (9)$$

where k is the wave number, $d_{s,s'}$ is the distance in meter between s and s' and $F_s(\theta_{s,s'}, \phi_{s,s'})$ is the radiation field pattern of feed antenna element s toward metamaterial unit cell s' calculated in (7). This equation models the spherical wave propagation from the antenna element s to the metamaterial unit cell s' composing the metasurface after the TX feed antenna. Note that (9) assumes that only a direct path between the antenna element and the metamaterial unit cell exists, and reflected or scattered paths are neglected. Next, $\boldsymbol{H}_{M_{TX}}$ and $\boldsymbol{H}_{M_{RX}}$ are phase-delaying diagonal matrices[6] designed to form co-phase waves to the beam angle θ, which is derived as follows:

$$kd_m \sin(\theta) + \psi_m + \psi_{ant} = 0 \quad (10)$$

where d_m is the distance between metamaterial unit cells, ψ_m is the phase delay induced by metamaterial unit cell m, and ψ_{ant} is the sum of phases of EM waves coming from the feed antenna calculated in (9). Eq. (10) implies that the summation of all phase offsets of a ray passing through an antenna and a metamaterial unit cell should have the same value for every metamaterial element m. Note that ψ_m contains the sum of phase offsets of $\boldsymbol{H}_{M_{TX}}$ and $\boldsymbol{H}_{M_{RX}}$. As mentioned above, d_m is designed to be less than half a wavelength; Specifically, which is set to one tenth of the wavelength in our proposed MLA design.

Finally, propagation channel $\boldsymbol{H}_{UMa}$ between TX and RX MLA is derived as a sum of line-of-sight (LOS) and non-line-of-sight (NLOS) components. The NLOS fast fading channel

[6] $\boldsymbol{H}_{M_{TX}} = \mathrm{diag}(e^{-jk\psi_1}, \ldots, e^{-jk\psi_M}) = \begin{bmatrix} e^{-jk\psi_1} & \cdots & 0 \\ 0 & \ddots & 0 \\ 0 & 0 & e^{-jk\psi_{M_T}} \end{bmatrix}$,
where each diagonal component ψ_m satisfies (10). Note that when there are multiple incoming radio waves from feed antenna array, ψ_{ant} should be the sum of all radio waves of antenna elements

$H^{NLOS}_{(u,s,n,m)}(t)$ is given in the 3GPP channel model [27] as follows:

$$\begin{aligned} &H^{NLOS}_{u,s,n,m}(t) \\ &= \sqrt{\frac{P_n}{M}} \begin{bmatrix} F_{rx,u,\theta}(\theta_{n,m,ZOA}, \phi_{n,m,AOA}) \\ F_{rx,u,\phi}(\theta_{n,m,ZOA}, \phi_{n,m,AOA}) \end{bmatrix} \\ &\quad \times \begin{bmatrix} \exp(j\Phi^{\theta\theta}_{n,m}) & \sqrt{\kappa^{-1}_{n,m}} \exp(j\Phi^{\theta\phi}_{n,m}) \\ \sqrt{\kappa^{-1}_{n,m}} \exp(j\Phi^{\phi\theta}_{n,m}) & \exp(j\Phi^{\phi\phi}_{n,m}) \end{bmatrix} \\ &\quad \times \begin{bmatrix} F_{tx,s,\theta}(\theta_{n,m,ZOA}, \phi_{n,m,AOA}) \\ F_{tx,s,\phi}(\theta_{n,m,ZOA}, \phi_{n,m,AOA}) \end{bmatrix} \exp\left(\frac{j2\pi \hat{r}^T_{rx,n,m} \bar{d}_{rx,u}}{\lambda_0}\right) \\ &\quad \times \exp\left(\frac{j2\pi \hat{r}^T_{tx,n,m} \bar{d}_{tx,s}}{\lambda_0}\right) \exp\left(\frac{j2\pi \hat{r}^T_{rx,n,m} \cdot \bar{v}}{\lambda_0} t\right) \end{aligned} \tag{11}$$

where P_n is the power of cluster n, $F_{rx,u,\theta}$ and $F_{rx,u,\phi}$ are vertical and horizontal radiation field pattern of RX antenna element u, respectively, $\{\phi^{\theta\theta}_{n,m}, \phi^{\theta\phi}_{n,m}, \phi^{\phi\theta}_{n,m}, \phi^{\phi\phi}_{n,m}\}$ are random initial phase for each ray m of each cluster n for four different polarization combination $(\theta\theta, \theta\phi, \phi\theta, \phi\phi)$, $F_{tx,s,\theta}$ and $F_{tx,s,\phi}$ are vertical and horizontal radiation field pattern of TX antenna element s, respectively, $\kappa_{n,m}$ is the cross polarization power ratio for each ray m of each cluster n, $\hat{r}_{rx,n,m}$ is the spherical unit vector with azimuth arrival angle $\phi_{n,m,AOA}$ and elevation arrival angle $\theta_{n,m,AOD}$, and $r_{tx,n,m}$ is the spherical unit vector with azimuth departure angle $\phi_{n,m,AOD}$ and elevation departure angle $\theta_{n,m,ZOD}$.

Likewise, the LOS fast fading channel $H^{LOS}_{u,s,1}(t)$ is given in the 3GPP channel model [27] as

$$\begin{aligned} &H^{LOS}_{u,s,1}(t) \\ &= \begin{bmatrix} F_{rx,u,\theta}(\theta_{n,m,ZOA}, \phi_{n,m,AOA}) \\ F_{rx,u,\phi}(\theta_{n,m,ZOA}, \phi_{n,m,AOA}) \end{bmatrix}^T \\ &\quad \times \begin{bmatrix} 1 & 0 \\ 0 & 1 \end{bmatrix} \begin{bmatrix} F_{tx,s,\theta}(\theta_{n,m,ZOA}, \phi_{n,m,AOA}) \\ F_{tx,s,\phi}(\theta_{n,m,ZOA}, \phi_{n,m,AOA}) \end{bmatrix} \\ &\quad \times \exp\left(-j2\pi \frac{d_{3D}}{\lambda_0}\right) \exp\left(\frac{j2\pi \hat{r}^T_{rx,LOS} \bar{d}_{rx,u}}{\lambda_0}\right) \\ &\quad \times \exp\left(\frac{j2\pi \hat{r}^T_{tx,LOS} \bar{d}_{tx,s}}{\lambda_0}\right) \exp\left(\frac{j2\pi \hat{r}^T_{rx,LOS} \cdot \bar{v}}{\lambda_0} t\right) \end{aligned} \tag{12}$$

Consequently, $\boldsymbol{H}^{UMa}_{u,s}$ is given by adding the LOS channel coefficient to the NLOS channel impulse response and scaling both terms according to the desired K-factor K_R as

$$\begin{aligned} H^{UMa}_{u,s}(\tau, t) = &\sqrt{\frac{1}{K_R + 1}} H^{NLOS}_{u,s}(\tau, t) \\ &+ \sqrt{\frac{K_R}{K_R + 1}} H^{LOS}_{u,s,1}(t) \delta(\tau - \tau_1) \end{aligned} \tag{13}$$

where $H^{NLOS}_{u,s}(\tau, t) = \sum_{n=1}^{N} \sum_{m=1}^{M} H^{NLOS}_{u,s,n,m}(t)$ for N clusters and M rays in a cluster [27].

IV. EVALUATION AND DISCUSSION

A. MEASUREMENT SETUP

Fig. 6 shows the measurement setup for the verification of beamforming gain of MLA. The aperture size of lens prototype was 50.4 mm × 50.4 mm which composed of 28 × 28 unit cells. The design of the lens prototype is considering the focal distance between the feed antenna and metamaterial lens and the beamwidth of the feed dipole antenna for the lens to fully utilize the transmitted power of the feed antenna, and detailed specification of metamaterial is equivalent to that utilized in [28]. A 1.6 dBi dipole antenna is used as a feed antenna to simulate beams from multiple feed antenna array with precoding $p \in \{e_1, e_2, e_3, e_4\}$, in 3, where e_n is the unit vector with one in nth element. The distance between feed antenna and metamaterial lens is set to 2 cm, which is approximately $2\lambda_0$, where λ_0 is the free-space wavelength at 28 GHz carrier frequency. The metamaterial lens prototype is designed to refract EM waves in 28 GHz and has the focal distance of 2 cm to meet the far field condition of the feed antenna. It was fabricated by printing metal unit cells of different sizes on a dielectric substrate at $\lambda_0/2$ intervals. By having unit cells of different structures, different phases can be applied to incoming EM waves as described in (1). A horn antenna fixed to the rotator is used as the RX antenna to measure the lens gain.

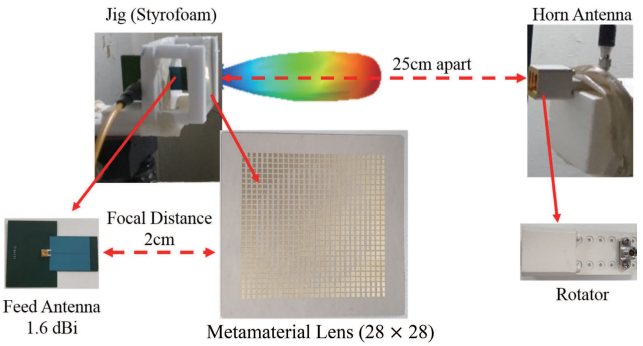

FIGURE 6. Measurement setup. The prototype of the metamaterial lens is located in front of the dipole antenna for TX, and a horn antenna for RX fixed to the rotator is positioned to measure the radiation patterns..

B. VERIFICATION OF THE PROPOSED MLA MODELING

Fig. 7a and 7b show the measurement and simulation results of Fig. 6. Each plot in Fig. 7a is the radiation pattern measured by rotating the RX antenna from −90° to 90°. The measurements show that the maximum gain of 14 dB can be achieved by the antenna selected by precoding. For the other antennas, the boresight direction of radiation pattern moves since the location of feed antenna is increased. As shown in left inset of Fig. 7a, feed antenna moves to $1\lambda_0(\approx 1cm)$ further from the focal axis of metamaterial lens to change the incident beam direction. Then, in this experiment, the absolute distance between lens and antenna increases. As the distance increases, the received power of the metamaterial unit cells decreases, following the channel model in (9).

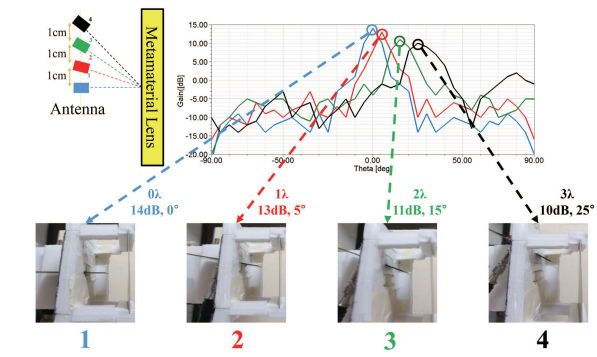

(a) Measurement

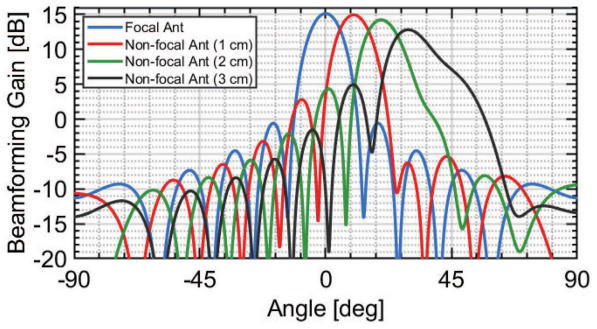

(b) Simulation Result

FIGURE 7. Comparison between (a) measurement and (b) simulation of beamforming gain of metasurface. The non-focal antenna gains decrease due to the misaligned phase offsets of metamaterial lens fine-tuned for the focal (blue line) antenna.

Fig. 7b simulate the array pattern after MLA by modeling (9) and (10). As shown in Fig. 7, the simulation shows similar results verifying that the proposed meta channel model agrees well with the experimental results with the MLA prototype.

C. MULTI-BEAM METAMATERIAL LENS DESIGN

Fig. 8a shows an example of received beam patterns along the lens aperture from 4×1 linear cross-polarized feed antennas. Note that only the one-dimensional MLA designs are considered to evaluate the azimuth beam pattern. The feed antennas are separated from each other by $0.5\lambda_0$. The metamaterial lens radius is set to $8\lambda_0$, and the unit cells are arranged linearly apart from each other by $0.1\lambda_0$, so the total number of metamaterial unit cells S' is set to 161. In order to tilt beam direction, discrete Fourier transform (DFT)-based beamforming vector 8-TX codebook design was utilized, i.e., $\boldsymbol{P} = \boldsymbol{W}^{(k)}_{(m,n)}$ where k is the channel rank. For example, when the rank is one, i.e., for $k = 1$, $\boldsymbol{W}^{(1)}_{(m,n)} = 1/\sqrt{8k}\,[\,\nu_m\ \phi_n\nu_m\,]^T$, $\nu_m = [\,1\ e^{j2\pi m/32}\ e^{j4\pi m/32}\ e^{j6\pi m/32}\,]^T$ and $\phi_n = e^{j\pi n/2}$ for $n \in \{0, 1, 2, 3\}$. Among the various beamforming vectors, only five codebook patterns are realized in Fig. 8a, and the received beam patterns are depicted to simplify metamaterial lens design in Fig. 8b. Note that not only the five beams, all other beams created by DFT-based beamforming vector defined in new radio (NR) release 15 can be radiated toward

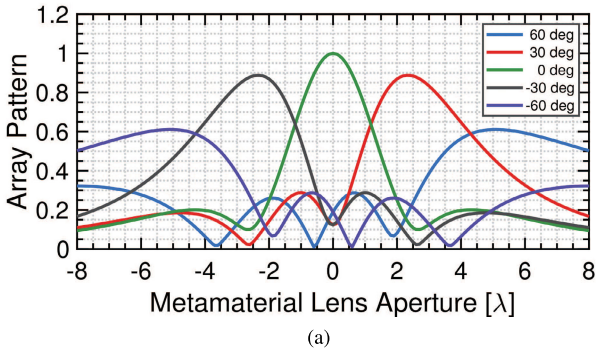

(a)

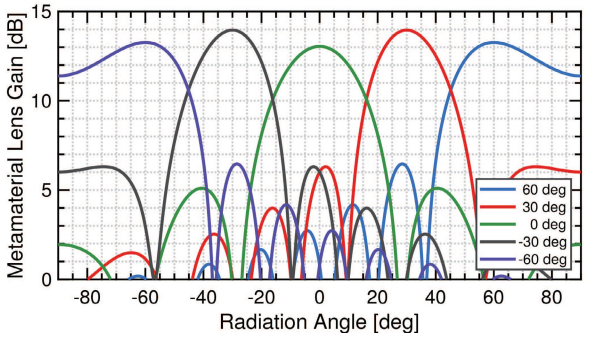

(b)

FIGURE 8. (a) Received beam pattern on the metamaterial lens and (b) metamaterial lens gain along the radiation angle.

the large-aperture metamaterial lens by changing precoding $\boldsymbol{P}$. For the proposed MLA design, we separate the lens area into five sub-areas that have respective phase offset values to preserve the beam directions from linear feed antenna.

Fig. 8b shows lens gains from the designed metamaterial lens from the initial beams of Fig. 8a. The metamaterial lens is composed of 161 unit cells with $0.1\lambda_0$ size, and these are designed to emit co-phased beams toward the received direction with gains of up to 14 dB.[7] Note that the meta channel in (2) is utilized to design the co-phased beams. By transmitting or receiving spatially different beams using one large-aperture MLA, multi-layer transmission is possible, and the aforementioned meta channel is required again in order to design a high-gain MLA structure.

D. SYSTEM-LEVEL SIMULATION RESULTS

Fig. 9 shows the two-tier BS and UE deployment for the system-level simulation (SLS). The zero-tier BS is located at the center of Fig. 9, and 6 BSs are located adjacent to the zero-tier BS constituting the first-tier. Next, 12 BSs surround the first-tier BSs, configuring second-tier cell coverage. The two-tier cell deployment is a widely accepted layout for SLS since it can examine the network performances for cell-edge users such as throughput, fairness, etc. Channels between 19 BSs and 570 UEs are generated with the feed antenna

[7]Note that mutual coupling between elements in a MIMO structure reduces radiation efficiency, and various methods exist for suppressing mutual coupling in a MIMO antenna [14], [29]. In this article, the coupling loss is assumed to be completely mitigated.

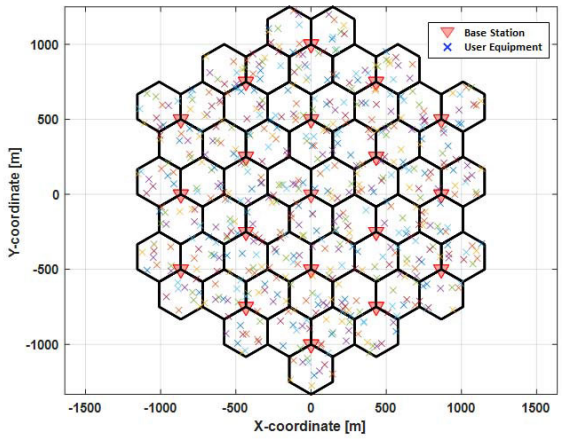

FIGURE 9. Two-tier cell deployment for system-level simulation.

TABLE 1. System-level simulation parameters.

Parameter	Value
Standardization	NR Release 15
Channel Model	TR 38.901
Channel Scenario	Urban Macro (UMa)
Cell Deployment	Two-tier Hexagonal (19 cells, 3sectors/cell)
Number of UEs per macro sites	10 (570 UEs total)
Carrier Frequency	28 GHz (FR2)
Subcarrier Spacing	60 kHz
Bandwidth	50 MHz
Number of Resource Blocks	66
Transmit Time Interval (TTI)	0.25 ms
UE speed	Indoor: 3 km/h Outdoor: 30 km/h
Polarization	Cross-polarized
Number of panels in column	1
Number of panels in row	1
Antenna elements in column	1, 8
Antenna elements in row	4, 8
Lens radius	8
Number of lens unit cells	161
Max. Directional Gain	8 dBi at BS 5 dBi at UE

array and MLA design proposed in Section III and IV. For each 3-sectorized cell, 10 UEs are distributed uniformly, and move 3 km/h or 30 km/h for indoor and outdoor condition for each transmit time interval (TTI). The parameters for SLS and antenna configuration are tabulated in Table 1. Note that the number of TX and RX antenna elements in rows and columns are changed to see the joint impact of MLA and MIMO operation.

Fig. 10 shows the cumulative distribution function (CDF) of per-UE throughput. UE throughputs are calculated based on modulation and coding scheme (MCS) level, transport

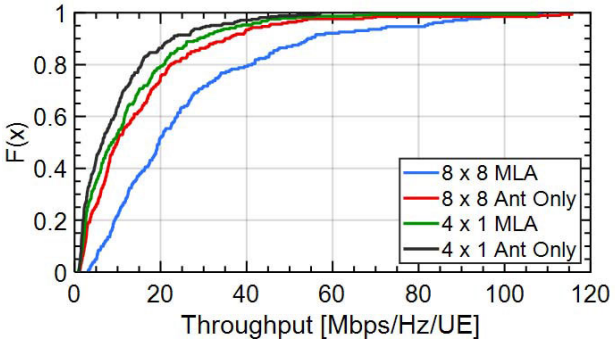

FIGURE 10. Cumulative distribution function of UE throughput.

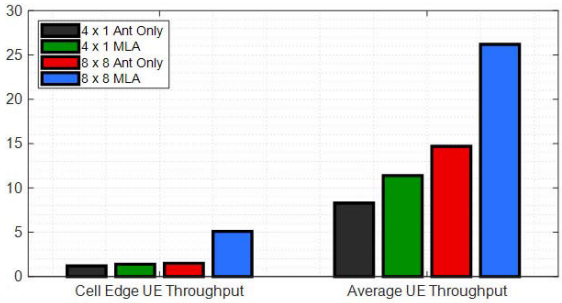

FIGURE 11. Cell edge UE (left) and average (right) UE throughput.

blocks size and spectral efficiency on each TTI. Simulations were performed for up to 1,000 TTIs and the initial 20% was set as a warm-up time and excluded from the results. As shown in Fig. 10, the case of MLA with 8×8 feed antennas shows the highest throughput values on the given deployment. The results show that the lens antenna can achieve much higher throughput due to spatial multiplexing and antenna diversity effects than when using the MIMO antenna array.

Fig. 11 shows the statistical results of cell edge UE throughput and average UE throughput. The cell edge UE throughput is defined as the 5th percentile point of the CDF of user throughput. In particular, the cell edge throughput has been dramatically improved because the signal-to-noise ratio (SNR) is improved due to the lens gain as well as the MIMO antenna. It can therefore be transmitted with a high MCS in MLA cases, resulting in high throughput for both of cell edge UEs and average UEs.

V. CONCLUSION

In this article, we have proposed a large-aperture MLA design for multi-layer transmission for future wireless communication system such as 6G. Based on the theoretic background of generalized law of refraction, the metamaterial unit cells are modeled and fabricated to focus dispersive EM waves in a designated direction. Based on the 28×28 lens prototype, this article shows that a single large-aperture MLA can achieve beam gain of up to 14 dB compared to the case without a lens. Measurement and simulation results corroborated that the proposed meta channel properly reflects the properties of the metamaterial lens forming multiple beam patterns from

multiple feed antenna elements and the subsequent beamforming gains after the metamaterial lens.

Using the proposed channel model and MLA designs, we have shown that multi-layer transmissions through MLA are also possible, which results in higher performance than the current MIMO antenna method in terms of throughput for cell edge UE and average UE [30], [31]. In particular, we demonstrate through SLS that the throughput gain of both average UE and cell edge UE increases with the improved beam gain of the proposed MLA. For example, an 8×8 MIMO antenna with the proposed metamaterial lens achieves more than 25 Mbps/Hz/UE throughput, whereas an 8×8 antenna-only system achieves merely 15 Mbps/Hz/UE for average UE throughput. In a reality where it is difficult to make several metamaterial lenses and to experiment with the actual propagation channel environments, the proposed model is expected to be of great help in quickly grasping the applicability of metamaterial lenses.

As mentioned earlier, despite the attractive wide bandwidth, there are several problems (limited hardware, RF loss, and high attenuation) to be addressed in order to use mmWave or THz bands in 6G cellular networks. In this situation, the proposed large-aperture MLA can be an effective solution that goes beyond the chronic limitations on mmWave and THz band. In addition, since the size of the metamaterial unit cell corresponds to the wavelength of the EM wave, as the frequency increases, more metamaterial unit cells can be embedded within the same aperture of the metamaterial lens, resulting in increased lens gain.

Note that advanced studies on programmable metamaterial which can adaptively change their phase shifting properties have been reported in recent years [32]–[35]. For example, one way to obtain programmable metamaterial is to introduce a varactor into unit cells [35]. The applied DC voltage makes a varactor act as an adjustable capacitor and controls the effective refractive index by influencing the resonance [36]. The programmable metamaterials are expected to provide a new degree of freedom for beam steering as well as massive MIMO operations based on our proposed MLA structure, so it will bring another innovation to increase system efficiency in future 6G wireless communication systems.

REFERENCES

[1] J. G. Andrews, S. Buzzi, W. Choi, S. V. Hanly, A. Lozano, A. C. Soong, and J. C. Zhang, "What will 5G be?" *IEEE J. Sel. Areas Commun.*, vol. 32, no. 6, pp. 1065–1082, Jun. 2014.

[2] T. S. Rappaport, Y. Xing, O. Kanhere, S. Ju, A. Madanayake, S. Mandal, A. Alkhateeb, and G. C. Trichopoulos, "Wireless communications and applications above 100 GHz: Opportunities and challenges for 6G and beyond," *IEEE Access*, vol. 7, pp. 78729–78757, 2019.

[3] M. Shafi, J. Zhang, H. Tataria, A. F. Molisch, S. Sun, T. S. Rappaport, F. Tufvesson, S. Wu, and K. Kitao, "Microwave vs. millimeter-wave propagation channels: Key differences and impact on 5G cellular systems," *IEEE Commun. Mag.*, vol. 56, no. 12, pp. 14–20, Dec. 2018.

[4] T. S. Rappaport, F. Gutierrez, Jr., E. Ben-Dor, J. N. Murdock, Y. Qiao, and J. I. Tamir, "Broadband millimeter-wave propagation measurements and models using adaptive-beam antennas for outdoor urban cellular communications," *IEEE Trans. Antennas Propag.*, vol. 61, no. 4, pp. 1850–1859, Apr. 2013.

[5] L. Lu, G. Y. Li, A. L. Swindlehurst, A. Ashikhmin, and R. Zhang, "An overview of massive MIMO: Benefits and challenges," *IEEE J. Sel. Topics Signal Process.*, vol. 8, no. 5, pp. 742–758, Oct. 2014.

[6] O. Quevedo-Teruel, M. Ebrahimpouri, and F. Ghasemifard, "Lens antennas for 5G communications systems," *IEEE Commun. Mag.*, vol. 56, no. 7, pp. 36–41, Jul. 2018.

[7] Y. Zeng, R. Zhang, and Z. N. Chen, "Electromagnetic lens-focusing antenna enabled massive MIMO: Performance improvement and cost reduction," *IEEE J. Sel. Areas Commun.*, vol. 32, no. 6, pp. 1194–1206, Jun. 2014.

[8] D.-H. Kwon and D. H. Werner, "Transformation electromagnetics: An overview of the theory and applications," *IEEE Antennas Propag. Mag.*, vol. 52, no. 1, pp. 24–46, Feb. 2010.

[9] S. Li, Z. N. Chen, T. Li, F. H. Lin, and X. Yin, "Characterization of metasurface lens antenna for sub-6 GHz dual-polarization full-dimension massive MIMO and multibeam systems," *IEEE Trans. Antennas Propag.*, vol. 68, no. 3, pp. 1366–1377, Mar. 2020.

[10] M. Jiang, Z. N. Chen, Y. Zhang, W. Hong, and X. Xuan, "Metamaterial-based thin planar lens antenna for spatial beamforming and multi-beam massive MIMO," *IEEE Trans. Antennas Propag.*, vol. 65, no. 2, pp. 464–472, Feb. 2017.

[11] M. Alibakhshikenari, B. S. Virdee, L. Azpilicueta, M. Naser-Moghadasi, M. O. Akinsolu, C. H. See, and B. Liu, "A comprehensive survey of 'metamaterial transmission-line based antennas: Design, challenges, and applications,'" *IEEE Access*, vol. 8, pp. 144778–144808, 2020.

[12] M. Alibakhshikenari, B. S. Virdee, P. Shukla, N. O. Parchin, L. Azpilicueta, C. H. See, R. A. Abd-Alhameed, F. Falcone, I. Huynen, and T. A. Denidni, "Metamaterial-inspired antenna array for application in microwave breast imaging systems for tumor detection," *IEEE Access*, vol. 8, pp. 174667–174678, 2020.

[13] M. Alibakhshikenari, B. S. Virdee, P. Shukla, Y. Wang, L. Azpilicueta, M. Naser-Moghadasi, C. H. See, I. Elfergani, C. Zebiri, R. A. Abd-Alhameed, I. Huynen, J. Rodriguez, T. A. Denidni, F. Falcone, and E. Limiti, "Impedance bandwidth improvement of a planar antenna based on metamaterial-inspired T-matching network," *IEEE Access*, vol. 9, pp. 67916–67927, 2021.

[14] M. Alibakhshikenari, F. Babaeian, B. S. Virdee, S. Aïssa, L. Azpilicueta, and C. H. See, "A comprehensive survey on 'various decoupling mechanisms with focus on metamaterial and metasurface principles applicable to SAR and MIMO antenna systems,'" *IEEE Access*, vol. 8, pp. 192965–193004, 2020.

[15] C. L. Holloway, E. F. Kuester, J. A. Gordon, J. O'Hara, J. Booth, and D. R. Smith, "An overview of the theory and applications of metasurfaces: The two-dimensional equivalents of metamaterials," *IEEE Antennas Propag. Mag.*, vol. 54, no. 2, pp. 10–35, Apr. 2012.

[16] N. Yu, P. Genevet, M. A. Kats, F. Aieta, J.-P. Tetienne, F. Capasso, and Z. Gaburro, "Light propagation with phase discontinuities: Generalized laws of reflection and refraction," *Science*, vol. 334, no. 6054, pp. 333–337, Oct. 2011.

[17] N. Yu and F. Capasso, "Flat optics with designer metasurfaces," *Nature Mater.*, vol. 13, no. 2, pp. 139–150, Jan. 2014.

[18] E. Erfani, M. Niroo-Jazi, and S. Tatu, "A high-gain broadband gradient refractive index metasurface lens antenna," *IEEE Trans. Antennas. Propag.*, vol. 64, no. 5, pp. 1968–1973, May 2016.

[19] T. Li and Z. N. Chen, "Miniaturized metasurface unit cell for microwave metalens antennas," in *Proc. Int. Conf. Electromagn. Adv. Appl. (ICEAA)*, Sep. 2017, pp. 980–983.

[20] Z. Li, J. Su, and Z. Li, "Design of high-gain lens antenna based on phase-gradient metasurface," in *Proc. 11th Int. Symp. Antennas, Propag. EM Theory (ISAPE)*, Oct. 2016, pp. 135–138.

[21] H. Li, G. Wang, H.-X. Xu, T. Cai, and J. Liang, "X-band phase-gradient metasurface for high-gain lens antenna application," *IEEE Trans. Antennas Propag.*, vol. 63, no. 11, pp. 5144–5149, Nov. 2015.

[22] A. Vallecchi, F. Capolino, and A. G. Schuchinsky, "2-D isotropic effective negative refractive index metamaterial in planar technology," *IEEE Microw. Wireless Compon. Lett.*, vol. 19, no. 5, pp. 269–271, May 2009.

[23] C. G. Parazzoli, R. B. Greegor, and M. Tanielian, "Development of negative index of refraction metamaterials with split ring resonators and wires for RF lens applications," in *Physics of Negative Refraction and Negative Index Materials*. Cham, Switzerland: Springer, 2007, pp. 261–329. [Online]. Available: https://link.springer.com/chapter/10.1007/978-3-540-72132-1_11 and https://link.springer.com/book/10.1007/978-3-540-72132-1

[24] Z. Hamzavi-Zarghani, A. Yahaghi, and L. Matekovits, "Reconfigurable metasurface lens based on graphene split ring resonators using Pancharatnam–Berry phase manipulation," *J. Electromagn. Waves Appl.*, vol. 33, no. 5, pp. 572–583, 2019.
[25] Y. Su and Z. N. Chen, "A flat dual-polarized transformation-optics beam-scanning Luneburg lens antenna using PCB-stacked gradient index metamaterials," *IEEE Trans. Antennas Propag.*, vol. 66, no. 10, pp. 5088–5097, Oct. 2018.
[26] J. Oh, "Millimeter-wave short-focus thin lens employing disparate filter arrays," *IEEE Antennas Wireless Propag. Lett.*, vol. 15, pp. 1446–1449, 2016.
[27] *Study on Channel Model for Frequencies From 0.5 to 100 GHz*, document 38.901, 2020, rel 16.
[28] I. Yoon and J. Oh, "Millimeter-wave thin lens using multi-patch incorporated unit cells for polarization-dependent beam shaping," *IEEE Access*, vol. 7, pp. 45504–45511, 2019.
[29] U. Qureshi, M. U. Khan, M. S. Sharawi, S. N. Burokur, and R. Mittra, "Field decorrelation and isolation improvement in an MIMO antenna using an all-dielectric device based on transformation electromagnetics," *Sensors*, vol. 21, no. 22, p. 7577, Nov. 2021.
[30] Y. Liu, G. Pan, H. Zhang, and M. Song, "On the capacity comparison between MIMO-NOMA and MIMO-OMA," *IEEE Access*, vol. 4, pp. 2123–2129, 2016.
[31] E. Khorov, I. Levitsky, and I. F. Akyildiz, "Current status and directions of IEEE 802.11be, the future Wi-Fi 7," *IEEE Access*, vol. 8, pp. 88664–88688, 2020.
[32] H. Yang, X. Cao, F. Yang, J. Gao, S. Xu, M. Li, X. Chen, Y. Zhao, Y. Zheng, and S. Li, "A programmable metasurface with dynamic polarization, scattering and focusing control," *Sci. Rep.*, vol. 6, no. 1, pp. 1–11, Oct. 2016.
[33] T. J. Cui, M. Q. Qi, X. Wan, J. Zhao, and Q. Cheng, "Coding metamaterials, digital metamaterials and programmable metamaterials," *Light: Sci. Appl.*, vol. 3, no. 10, p. e218, Oct. 2014.
[34] C. Liaskos, S. Nie, A. Tsioliaridou, A. Pitsillides, S. Ioannidis, and I. Akyildiz, "A new wireless communication paradigm through software-controlled metasurfaces," *IEEE Commun. Mag.*, vol. 56, no. 9, pp. 162–169, Sep. 2018.
[35] F. Liu, A. Pitilakis, M. S. Mirmoosa, O. Tsilipakos, X. Wang, A. C. Tasolamprou, S. Abadal, A. Cabellos-Aparicio, E. Alarcon, C. Liaskos, N. V. Kantartzis, M. Kafesaki, E. N. Economou, C. M. Soukoulis, and S. Tretyakov, "Programmable metasurfaces: State of the art and prospects," in *Proc. IEEE Int. Symp. Circuits Syst. (ISCAS)*, May 2018, pp. 1–5.
[36] T. Jiang, Z. Wang, D. Li, J. Pan, B. Zhang, J. Huangfu, Y. Salamin, C. Li, and L. Ran, "Low-DC voltage-controlled steering-antenna radome utilizing tunable active metamaterial," *IEEE Trans. Microw. Theory Techn.*, vol. 60, no. 1, pp. 170–178, Jan. 2012.

JAEHYUN LEE (Member, IEEE) received the B.S. degree in electrical engineering from the Pohang University of Science and Technology, Pohang, South Korea, in 2012, and the joint M.S. and Ph.D. degree in electrical engineering from Seoul National University, Seoul, South Korea, in 2018.

Since 2018, he has been working as a Staff Engineer with the 6G Research Team, Advanced Communications Research Center, Samsung Research, Samsung Electronics, Seoul. His current research interests include next-generation wireless communication systems (6G), metamaterial RF front-end, wireless propagation channel measurement and modeling, machine learning and artificial intelligence for wireless communication, millimeter-wave and terahertz communication, and the ray-tracing simulation of cellular networks.

HOGYEOM KIM (Graduate Student Member, IEEE) received the B.S. degree from Inha University, South Korea, in 2016. He is currently pursuing the M.S. degree with Seoul National University, South Korea. He was a Research Engineer with the Millimeter Multiscale Wave Laboratory, Inha University. His current research interests include transmit array antennas for 5G communication and millimeter-wave radar systems.

JUNGSUEK OH (Senior Member, IEEE) received the B.S. and M.S. degrees from Seoul National University, South Korea, in 2002 and 2007, respectively, and the Ph.D. degree from the University of Michigan at Ann Arbor, in 2012.

From 2007 to 2008, he was with Korea Telecom as a Hardware Research Engineer, working on the development of flexible RF devices. In 2012, he was a Postdoctoral Research Fellow with the Radiation Laboratory, University of Michigan. From 2013 to 2014, he was a Staff RF Engineer with Samsung Research America, Dallas, where he is working as a Project Leader of the 5G/millimeter-wave antenna systems. From 2015 to 2018, he was a Faculty Member with the Department of Electronic Engineering, Inha University, South Korea. He is currently an Assistant Professor with the School of Electrical and Computer Engineering, Seoul National University. He has published more than 40 technical journals and conference papers. His research interests include mmWave beam focusing/shaping techniques, antenna miniaturization for integrated systems, and radio propagation modeling for indoor scenarios. He has served as a TPC Member and the Session Chair for the IEEE AP-S/USNC-URSI and ISAP. He was a recipient of the 2011 Rackham Predoctoral Fellowship Award at the University of Michigan. He has served as a Technical Reviewer for IEEE TRANSACTIONS ON ANTENNAS AND PROPAGATION and IEEE ANTENNA AND WIRELESS PROPAGATION LETTERS.